ACS APPLIED NANO MATERIALS
Cite This: ACS Appl. Nano Mater. 2018, 1, 595−608
Article
www.acsanm.org

Folate-Conjugated Halloysite Nanotubes, an Efficient Drug Carrier, Deliver Doxorubicin for Targeted Therapy of Breast Cancer

Yan-Ping Wu,[§,†] Jing Yang,[§,‡] Hua-Ying Gao,[†] Yan Shen,[‡] Lingxiang Jiang,[‡] Changren Zhou,[‡] Yi-Fang Li,[†] Rong-Rong He,[*,†] and Mingxian Liu[*,‡]

[†]Guangdong Province Key Laboratory of Pharmacodynamic Constituents of TCM and New Drugs Research, College of Pharmacy and [‡]Department of Materials Science and Engineering, Jinan University, Guangzhou 510632, China

Supporting Information

ABSTRACT: To carry doxorubicin (DOX) on breast cancer site effectively, halloysite nanotubes conjugated with poly(ethylene glycol) and folate (HNTs-PEG-FA) is designed as a targeted drug delivery system. Halloysite nanotubes (HNTs) are shortened to ∼200 nm by ultrasonic scission and functionalized with amide groups to conjugate with *N*-hydroxylsuccinimide-polyethylene glycol carboxylic acid (NHS-PEG-COOH) and folate (FA). DOX@HNTs-PEG-FA is prepared by loading DOX on HNTs-PEG-FA via physical adsorption. The sustained and controlled release of DOX from DOX@HNTs-PEG-FA is up to 35 h in an acidic environment (pH 5.3). DOX@HNTs-PEG-FA, performed as a new nanodelivery system, shows significant inhibition of proliferation and induction of death in MCF-7 cells with positive FA receptor but not in L02 cells with negative FA receptor. Results of acridine orange/ethidium bromide and flow cytometric assay indicate that DOX@HNTs-PEG-FA induces cell death through apoptosis. Compared to the same dose of DOX, DOX@HNTs-PEG-FA generates more reactive oxygen species (ROS) in MCF-7 cells, which lead to mitochondrial damage and apoptosis. Furthermore, with fluorescence images and transmission electron microscopy, uptake of DOX@HNTs-PEG-FA by tumor cells is both through endocytosis and direct penetration mechanism. The in vivo antibreast cancer activity of DOX@HNTs-PEG-FA is further confirmed in 4T1-bearing mice. In contrast to DOX, DOX@HNTs-PEG-FA effectively reduces heart toxicity and inhibits solid tumor growth with higher cleaved caspase-3 protein level in tumor tissue of 4T1-bearing mice. DOX@HNTs-PEG-FA reveals a higher DOX fluorescence intensity in tumor tissue than in other normal tissues including heart, spleen, lung, and kidney at different time points. All these results suggest that FA-conjugated HNTs may be designed to be a novel drug delivery system for targeted therapy of breast cancer via intravenous injection.

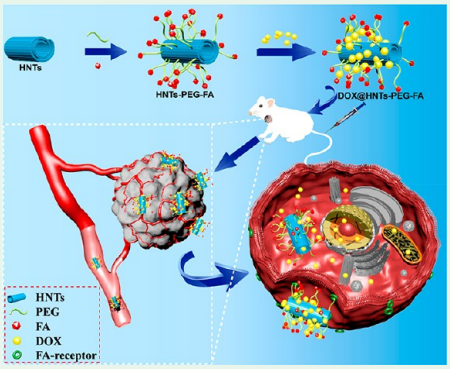

KEYWORDS: *halloysite, nanotube, targeting therapy, cancer, folate, intravenous injection*

1. INTRODUCTION

In cancer treatment options, chemotherapy is the most common therapy in the clinic. However, chemotherapy drugs do not have the ability to recognize cancer cells from normal cells due to lack of selectivity, resulting in lots of side effects. Doxorubicin (DOX) is an effective and widely used chemotherapeutic agent in different cancers.[1] However, its short biological half-period and nonspecific distribution lead to significant side effects such as pain, nausea, vomiting, diarrhea, loss of appetite, congestive heart failure, and low blood counts.[2,3] Therefore, several nanocarriers were designed for targeting release of DOX to reduce its distribution in normal tissues.[4] DOX can be physically adsorbed on the nanoparticles or chemically conjugated to nanoparticles, which leads to a controlled release manner of the drug toward tumor sites. However, there are still some drawbacks for these synthesized nanoparticles, such as high cost, complicated synthesis process, high cytotoxicity, and hard to replicate. Therefore, it is significant to explore natural nanoparticles as anticancer drug carrier for targeting tumor therapy.

Compared with normal cells, tumor cells overexpress certain receptors and tumor-associated surface antigens. Therefore, the corresponding ligands or antibodies can be conjugated to drugs to improve their active identification and targeting ability to tumors, which can decrease the side effects as expected. Folate (FA) has been recognized as an important ligand for specific labeling of cancer cells because of the overexpression of FA receptors on the surface of several cancer cells.[5] FA receptor is nearly not expressed in normal tissues but overexpressed in many human tumors, including tumors of the ovary, uterus, endometrium, brain, kidney, cervical, rhinitis, colon, and breast.[6] Folate has numerous advantages over other targeting molecules, for example, relatively small molecular weight, no immunogenicity, better stability, higher affinity for receptors, easier modification of functional groups, ease of use, etc.[7] A series of nanomaterials, such as carbon nanomaterials,[8−10]

Received: October 25, 2017
Accepted: December 29, 2017
Published: December 29, 2017

DOI: 10.1021/acsanm.7b00087
ACS Appl. Nano Mater. 2018, 1, 595−608

Scheme 1. Schematic Illustration of Synthesis Procedure for DOX@HNTs-PEG-FA and the Targeting Release of DOX from HNTs-PEG-FA in the Tumor Cells

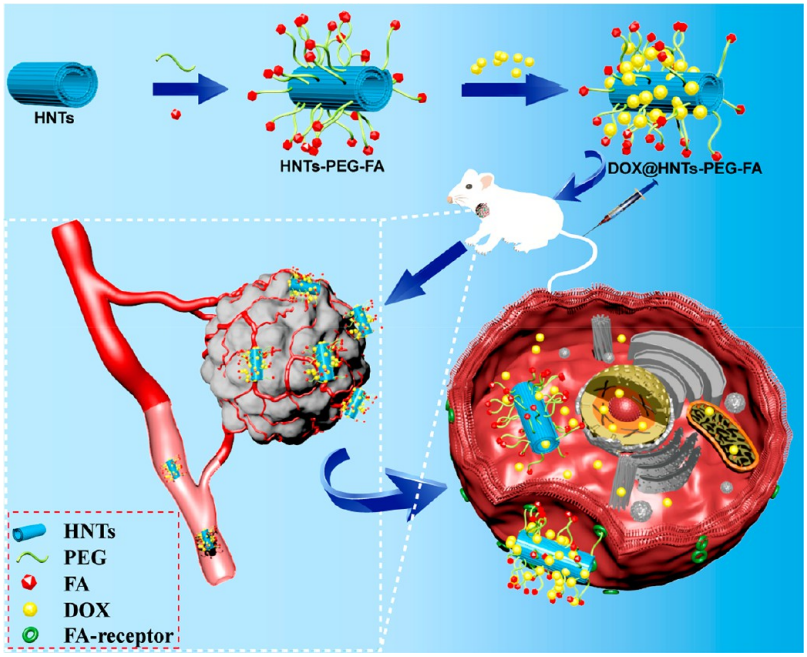

quantum dots,[11] and metal nanoparticles,[12] has been modified with FA for targeting imaging, diagnosis, and therapy applications of cancer.[13,14] For example, FA-functionalized gold nanoclusters can be used to target and image HeLa cancer cells.[5] FA-conjugated super-paramagnetic maghemite nanoparticles were also designed for the intracellular hyperthermia treatment of solid tumors.[15]

Halloysite nanotubes (HNTs) are naturally occurring aluminosilicate clay minerals that show promising applications in many high-tech fields. HNTs have a predominantly hollow tubular structure with length of 200−1000 nm and diameter of 50−70 nm. HNTs are a dominant mineral in newly formed volcanic ash soil and in the early weathering product of lateritic soil, which is widespread throughout the world. HNTs are formed by rolling up the kaolinite plates, so they have a formula of $Al_2Si_2O_5(OH)_4{\cdot}nH_2O$ similar to kaolinite.[16] The structure of HNTs features a main tubular morphology with the Al−OH layer forming inside of the tubes and the Si−O at the outside. Because of the empty tubular structure, HNTs have been identified as a "green" and environmentally available container for encapsulation of active agents in the area application of medical and chemical industries. The obvious advantages of HNTs, such as elongated shape, empty lumen, high adsorption ability, ease of dispersion within polymers, good biocompatibility, environmental friendliness, and abundant availability,[17−21] have gained significant attention in recent years. HNTs can capture molecules to the external and internal walls of tubes via adsorption, or the drugs can be loaded into lumen and intercalated between layers. Drugs released from HNTs usually last for several hours to days, depending on the molecular mass, interactions between drugs and HNTs, and the solubility of drugs in the release medium. For example, the poly(*N*-isopropylacrylamide) and chitosan grafted HNTs can be used as a novel drug carrier for curcumin delivery.[22,23] The dopamine-modified HNTs shows an excellent loading capacity,[24] and HNTs-based biomimetic porous microspheres possess an effective support for biomolecule immobilization.[25] Triazolium salts modified HNTs can also improve the antitumor effect of curcumin and cardanol when compared with the use of drugs alone. Chitosan oligosaccharide grafted HNTs (HNTs-*g*-COS) were designed as DOX carrier for treating breast cancer both in vitro and in vivo in our previous experiment. And the tumor inhibition ratio of DOX@HNTs-*g*-COS is 83%, while it is 46% for pristine DOX.[26] Different kinds of modified HNTs are designed for delivering anticancer drug either in vitro level or through intratumor injection, but few of them are designed for targeting therapy.

To further investigate the HNTs as anticancer drug carrier for targeting tumor therapy, HNTs conjugated with poly(ethylene glycol) and folate (HNTs-PEG-FA) were developed in this study. The length of the HNTs was first shortened to ∼200 nm by ultrasonic scission for increasing the endocytosis efficacy. Afterward, poly(ethylene glycol) (PEG) was conjugated to HNTs for prolonging their circulation time and controlling their dosing interval. FA was subsequently grafted onto HNTs to obtain tumor targeting system. The physical and chemical properties of HNTs-PEG-FA and the antitumor properties of DOX@HNTs-PEG-FA were investigated in vitro and in vivo. The release characteristics of DOX from the nanoparticles were analyzed. MCF-7 cells were chosen as the target cells due to their overexpression of FA receptors. The killing effect of drug loading modified HNTs on tumor cells was assessed by methyl thiazolyl tetrazolium (MTT) assay. The effect of the system on the growth curve of tumor cells was further investigated. Intracellular reactive oxygen species (ROS) level was also analyzed. Furthermore, the anticancer effect of DOX@HNTs-PEG-FA was confirmed in 4T1-bearing mice model via intravenous injection. As displayed in Scheme 1, DOX@HNTs-PEG-FA can effectively inhibit solid tumor growth by sustainable releasing DOX.

2. EXPERIMENTAL SECTION

2.1. Materials. HNTs with high purity were purchased from Guangzhou Runwo Materials Technology Co., Ltd. The elemental

DOI: 10.1021/acsanm.7b00087
ACS Appl. Nano Mater. 2018, 1, 595−608

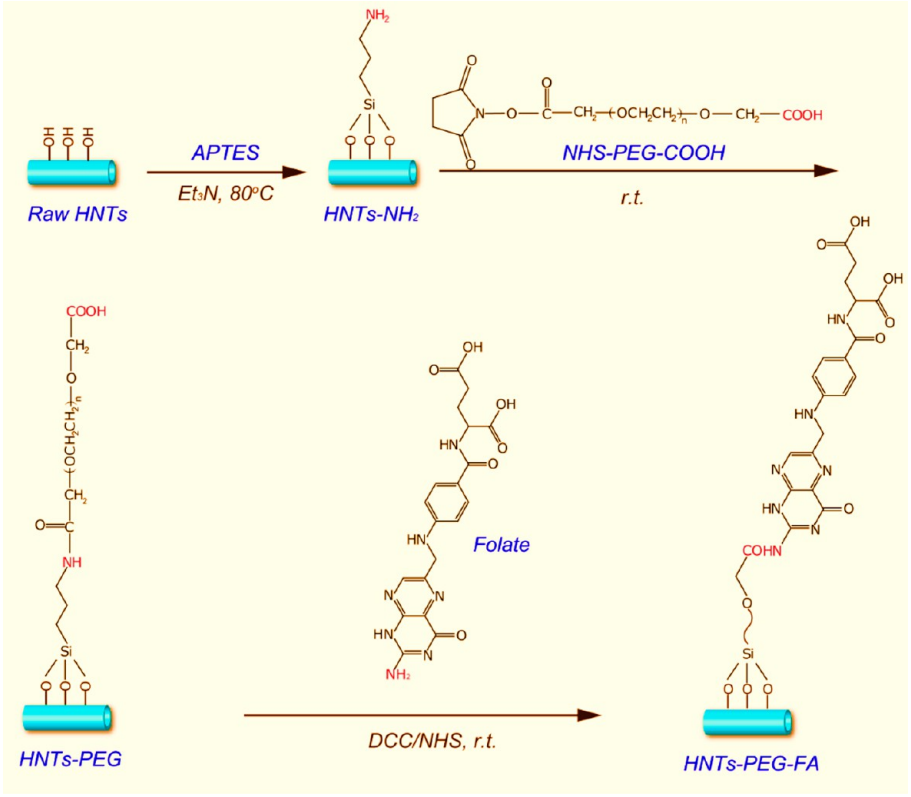

Figure 1. Schematic representation of HNTs-PEG-FA preparation.

composition of used HNTs by X-ray fluorescence (XRF) was determined as follows (wt %): SiO_2, 58.59; Al_2O_3, 40.57; MgO, 0.33; SO_3, 0.22; CaO, 0.14; Fe_2O_3, 0.07; Cl, 0.06; K_2O, 0.02. NHS-PEG-COOH (M_w, 5 kDa) was purchased from Shanghai Ponsure Biotechnology Co., Ltd. FA was purchased from Aladdin reagent (Shanghai) Co., Ltd. DOX was purchased from Nanjing Oddfoni Biological Technology Co. Ltd. Ultrapure water was produced from a Milli-Q water system. 3-Aminopropyltriethoxysilane (APTES), dicyclohexylcarbodiimide (DCC), and *N*-hydroxysuccinimide (NHS) were purchased from Aladdin. All other regents were used in analytical grade.

2.2. Synthesis of HNTs-PEG-FA. HNTs were shortened to ~200 nm in length according to the previous study.[27,28] The typical procedure was given as follows. Purified HNTs (1 g) were suspended in 50 mL of 3% poly(vinylpyrrolidone) aqueous solution by stirring for 30 min. Subsequently, the suspension was ultrasonically treated for 30 min at 550 W by ultrasonic cell disruptor (Scientz-II D, Ningbo Scientz Biotechnology Ltd). The suspensions were subsequently centrifuged at 5000 rpm for 45 min using ultracentrifuge (YNX-4000, Thermo Fisher Scientific Ltd). The supernatant was transferred to another 50 mL centrifuge tube and centrifuged again at 16 000 rpm for 5 min. The shortened HNTs were obtained by washing with ultrapure water and anhydrous ethanol alternatively and then lyophilized at −56 °C.

Then the short HNTs were conjugated with PEG and FA according to procedures shown in Figure 1. HNTs were first modified by APTES (silane coupling agent). The typical procedure was given below. HNTs (2 g) and APTES (0.2 mL) were added to 100 mL of toluene using triethylamine (0.1 mL) as catalyst under stirring at 80 °C for 24 h. To remove unreacted silane and obtain HNTs-NH_2, the precipitate was washed with ethanol, and HNTs-NH_2 was dried in vacuo for 12 h.[29] Then, NHS-PEG-COOH (0.015 g) was reacted with HNTs-NH_2 (1.5 g) using 50 mL of pure dimethyl sulfoxide (DMSO) as solvent under stirring for 24 h at room temperature. The product of HNTs-PEG was obtained by centrifugation. Lastly, HNTs-PEG (1 g) reacted with FA (0.01 g) via acylation reaction using 0.05 g of DCC/NHS as catalyst in 50 mL of DMSO. The products were washed with water and ethyl alcohol alternately three times. The final product was coded as HNTs-PEG-FA.

2.3. Characterization of HNTs-PEG-FA. Short HNTs and HNTs-PEG-FA aqueous dispersion (the concentration was 0.05%) were dropped onto holey carbon film on copper grids and observed using transmission electron microscopy (TEM; Philips Tecnai-10) under an accelerating voltage of 100 kV. Morphology of the two HNTs was also characterized by scanning electron microscopy (SEM; Philips LEO1530 VPSEM) at a voltage of 5 kV. Before the observation, a thin gold layer was sprayed on the surfaces. For atomic force microscopy (AFM) measurement, HNTs-PEG-FA mixture dispersion (ethanol/ultrapure water = 1/1) with the concentration of 0.005% was dropped in fresh mica slice and observed using AFM (Nanoscope IIIa Multimode, Veeco Co). The dynamic light scattering (DLS) analysis and zeta potential were measured at the pH of 7.4 (phosphate-buffered saline (PBS) buffer solution) by a Nano-ZS instrument (Malvern Instruments Ltd). Fourier transform infrared spectroscopy (FTIR) of the samples was analyzed by Bruker FTIR (Bruker Optics Inc) from 4000 to 400 cm^{-1} via the method of KBr pellet. The atomic percent of N, O, C, Si, and Al in HNTs-PEG-FA and the Brunauer−Emmett−Teller (BET) surface area of HNTs-PEG-FA were determined by X-ray photoelectron spectroscopy (XPS; Thermo Fisher Scientific) and automated surface area and pore size analyzer (3H-2000, BeiShiDe Instrument Technology Co. Ltd), respectively.

2.4. Drug Loading and Release. DOX was dissolved in ultrapure water (50 μg/mL), and then HNTs-PEG-FA (100 mg) was added into DOX solution (100 mL). After it was stirred in dark for 24 h, DOX-loaded HNTs-PEG-FA (DOX@HNTs-PEG-FA) was obtained by centrifuging at 10 000 rpm for 10 min and washing twice by ultrapure water. The supernatant liquid was reserved to measure the adsorbing capacity of HNTs-PEG-FA through ultraviolet−visible (UV/vis) spectroscopy. The DOX loaded with raw HNTs was also gained in the same procedure and was called DOX@HNTs. The loading efficiency was calculated as follows.

DOI: 10.1021/acsanm.7b00087
ACS Appl. Nano Mater. 2018, 1, 595−608

$$\text{loading efficiency}(\%) = \frac{\text{weight of loaded DOX}}{\text{total weight of nanoparticles and loaded DOX}} \times 100\%$$

DOX@HNTs-PEG-FA (20 mg) was added into PBS (2 mL) and phosphate buffer (2 mL) (pH = 5.3) with constant shaking at 37 °C in an Eppendorf tube, respectively. Supernatant liquid (1.5 mL) was obtained for measuring the released DOX from DOX@HNTs-PEG-FA via ultraviolet spectrophotometer after centrifugation (10 000 rpm, 2 min) at specific time. Then, the same volume of fresh PBS and phosphate buffer was supplied in the release medium.

2.5. Hemocompatibility of HNTs-PEG-FA. Fresh human blood (5 mL) was added into PBS solution (10 mL), and then the supernatant liquid was discarded after being centrifuged at 1000 rpm for 10 min. This procedure was repeated three times, and red blood cells (RBCs) were collected. Then, RBCs (320 μL) were added into PBS solution (1680 μL). RBCs suspension (25 μL) was further added into 500 μL of short HNTs and HNTs-PEG-FA PBS solution (1 mg/mL). After it was slightly vibrated, the RBCs suspension was incubated at 37 °C for 2 h. After incubation, all the samples were centrifuged at 1000*g* at 4 °C. The supernatant liquid (150 μL) was transferred to 96-well plate. The hemolysis ratio was determined by measuring the absorbance at 570 nm using a microplate reader. The positive control group was 100% hemolysis (in ultrapure water), and the negative control group was 0% hemolysis (in PBS solution). The hemolysis ratio was calculated using the following equation.

$$\text{hemolysis ratio}(\%) = \frac{\text{sample absorbance} - \text{negative control}}{\text{positive control} - \text{negative control}} \times 100\%$$

2.6. Animals Feeding and Cell Culture Conditions. Female BALB/c mice (seven weeks old) weighing 18−22 g were purchased from Guangdong Medical Laboratory Animal Center, with permission No. SCXK 2011-0015. All animal care and experimental procedures were approved by the Animal Care and Use Committee of Jinan University (Approval ID: 20150310001) and were in accordance with the National Institute of Health's Guide for the Care and Use of Laboratory Animals.

Human breast cancer cells (MCF-7), human normal liver cells (L02), human liver cancer cells (HepG2), and mouse breast cancer cells (4T1) were obtained from the Cell Bank of the China Academy of Sciences. MCF-7, L02, and HepG2 cells were cultured in Dulbecco's modified Eagle's medium (DMEM) (Gibco), 4T1 cells were maintained in RPMI 1640 (Gibco), containing 10% fetal bovine serum (FBS; Gibco) within a humidified atmosphere containing 5% CO_2 at 37 °C.

2.7. In Vitro Cytotoxicity Study. MCF-7, L02, and HepG2 cells (8.0×10^3 cells/well) were seeded in 96-well cell culture plates for 24 h and then incubated with the HNTs and HNTs-PEG-FA with concentrations of 0, 31.25, 62.5, 125, 250, and 500 μg/mL for 24 h. For drug-loaded nanoparticles, the cells were incubated with DOX, DOX@HNTs, and DOX@HNTs-PEG-FA at equivalent drug concentrations of 0, 0.625, 1.25, 2.5, 5, and 10 μg/mL for 24 h. MTT solution (5 mg/mL in PBS) was added into each well (20 μL/well). After 4 h, the culture medium was removed and replaced with DMSO (150 μL/well). To eliminate the influence of HNTs, HNTs-PEG-FA, DOX@HNTs, and DOX@HNTs-PEG-FA precipitation on the absorbance, supernatant liquid (100 μL) was transferred to a new 96-well cell culture plate for absorbance measurement. The DMSO solution was measured at 570 nm by a microplate reader.

Cellular behavior was further investigated by real-time cell analysis (RTCA) systems (iCELLigence, ACEA Biosciences Inc). RTCA was a label-free and real-time monitoring technology for cell proliferation, cell size/morphology, cell attachment quality, and cell invasion/migration, which could provide a phenotypic view of cellular behavior at an unprecedented level of detail. MCF-7, L02, and HepG2 cells (8×10^3 cells/well) were seeded in cell cultures with gold microelectrodes. The time when the cells attached and the medium replaced with fresh medium was described as 0 h in this study. The cells were incubated with DOX and DOX@HNTs-PEG-FA at different concentrations (0, 0.625, 1.25, 2.5, 5 μg/mL) at 22.2 h, respectively. The cell growth curve was recorded automatically by RTCA.

To observe the morphology of MCF-7 cells after treatment with different drugs, MCF-7 cells (2×10^4 cells/well) were seeded in 96-well plates for 24 h. Afterward, HNTs, HNTs-PEG-FA (the concentrations were 0, 31.25, 62.5, 125, 250, 500 μg/mL), DOX, and DOX@HNTs-PEG-FA (the concentrations were 0, 0.625, 1.25, 2.5, 5, and 10 μg/mL) were added to cells. After they were incubated for 24 h, cells were stained with 10 μL of mixtures of acridine orange (AO, 100 μg/mL) and ethidium bromide (EB, 100 μg/mL). Cell morphology was immediately examined under a fluorescent microscope (XDY-2, Liss Optical Instrument Ltd).

2.8. Cellular Uptake of DOX@HNTs-PEG-FA. To track the drug delivery in intracellular matrix, MCF-7 cells were cultured in cells in Petri dishes (1×10^4 cells) and treated with DOX and DOX@HNTs-PEG-FA (5 μg/mL) for 2, 4, 8, 12, and 24 h, respectively. Cells were fixed with 4% paraformaldehyde, stained with Alexa Fluor 488 Phalloidin (Molecular Probes) and imaged using a fluorescent microscope (XDY-2). To quantitatively evaluate the cellular uptake of DOX, MCF-7 cells were seeded in a six-well plate at a density of 1×10^5 cells/well and treated with DOX, DOX@HNTs, and DOX@HNTs-PEG-FA (DOX equivalent concentration 5 μg/mL) for 4 h, respectively. After the culture media was discarded, MCF-7 cells were washed with cold PBS three times and collected. DOX fluorescence intensity was analyzed by flow cytometer (FACS Gallios, Beckman).

MCF-7 cells were treated with HNTs-PEG-FA (250 μg/mL) for 8 h. Then, cells were collected and fixed in 2.5% glutaraldehyde in 0.1 M sodium cacodylate buffer (pH 7.4) for 1 h in room temperature. Cells were then post fixed 1 h in 2% osmium tetroxide with 3% potassium ferrocyanide. Afterward, the cells were stained with a 2% aqueous uranyl acetate solution and dehydrated through a graded series of alcohol. They were subsequently put into two changes of propylene oxide, a series of propylene/Epon dilutions, and embedded. The thin (70 nm) sections were cut on a Leica UC6 ultramicrotome (Leica Microsystems), and images were taken on a Philips Tecnai 10 TEM.

2.9. ROS Level Analysis. MCF-7 cells (5.0×10^4 cells/well) were cultured in 96-well plate or 2 cm Petri dish for 24 h. After they were incubated with dihydrorhodamine 123 for 0.5 h, cells were treated with PBS, DOX, DOX@HNTs, and DOX@HNTs-PEG-FA (DOX equivalent concentration 5 μg/mL), respectively. Finally, fluorescence intensity was detected at a special time by fluorescence microplate (Spectra Max M5, Bio-Tek) at 507 nm. Fluorescence images were obtained at a specific time using a fluorescent microscope (XDY-2).

2.10. Western Blot Analysis. Tumor tissue was lysed with RIPA buffer for western blotting analysis. Briefly, proteins (30 μg) were separated by 12% sodium dodecyl sulfate polyacrylamide gel electrophoresis (SDS-PAGE) and transferred onto a poly(vinylidene fluoride) membrane (Millipore). Membranes were blocked in 5% defatted milk and then incubated with primary antibodies (Cleaved caspase 3, Caspase 3, Bcl-2, or β-actin) overnight at 4 °C. Incubated with horseradish peroxidase-conjugated secondary antibodies, bound proteins were visualized by enhanced chemiluminescence (ECL; MultiSciences Biotech) and detected using Tannon 5200 Multi (Tannon). Blots were performed in triplicate, and band density was quantified by Quantity One software (Bio-Rad).

2.11. Cell Apoptosis Assay and Cell Cycle. MCF-7 cells were treated with PBS, DOX, DOX@HNTs, and DOX@HNTs-PEG-FA (equivalent concentration of DOX was 5 μg/mL) for 10 h in a six-well plate, respectively. After they were washed and centrifuged, the harvested cells were stained with Annexin V-FITC/propidium iodide (PI) Apoptosis Detection Kit for 15 min at room temperature and then were analyzed by a flow cytometer. In each experiment, 10 000 events per sample were recorded.

The effects of drugs on cell cycle distribution were further examined by flow cytometry. MCF-7 cells were separately treated with PBS, DOX, DOX@HNTs, and DOX@HNTs-PEG-FA (equivalent concentration of DOX was 5 μg/mL) for 24 h. Subsequently, cells were collected and fixed with 75% ethanol overnight at −20 °C. The fixed

DOI: 10.1021/acsanm.7b00087
ACS Appl. Nano Mater. 2018, 1, 595−608

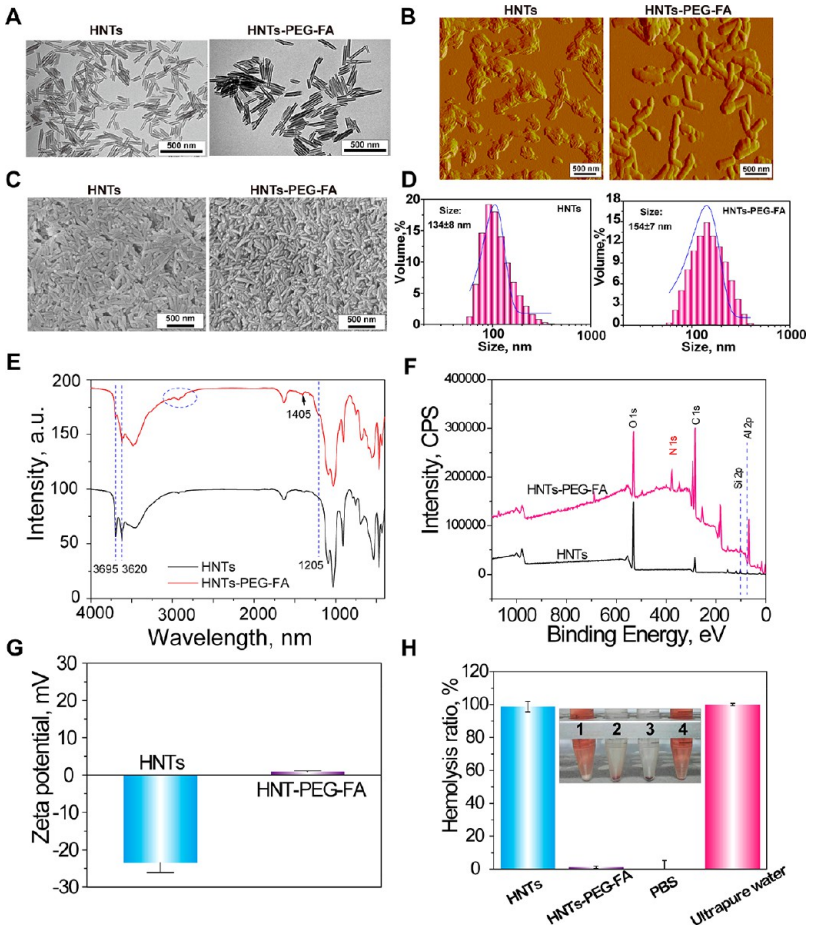

Figure 2. Characterization of short HNTs and HNTs-PEG-FA. (A) TEM, (B) AFM, (C) SEM, (D) DLS, (E) FTIR spectra, (F) XPS spectra, (G) zeta potentials, and (H) hemolysis ratio ((1) HNTs, (2) HNTs-PEG-FA, (3) PBS, (4) Ultrapure water).

cells were then stained with PI for ~1 h in darkness. At last, the stained cells were measured with flow cytometer, and 10 000 events per sample were recorded for each experiment.

2.12. In Vivo Antitumor Efficiency and Systemic Toxicity. The antitumor efficiency of DOX@HNTs-PEG-FA was studied in 4T1-bearing mice. To establish 4T1-bearing mice, 4T1 cells in a 1 × 10^6 cells suspension (200 μL) were injected into the second mammary fat pad of BALB/c mice. When tumor volume reached ~50 mm^3, the mice were randomly allocated into five groups (Control, HNTs, HNTs-PEG-FA, DOX, and DOX@HNTs-PEG-FA, n = 6). The mice were intravenously injected twice a week for three weeks with 200 μL of saline, HNTs, HNTs-PEG-FA, DOX (5 mg/kg), and DOX@HNTs-PEG-FA (5 mg DOX equiv/kg), respectively. The dose of DOX was chosen according to the previous researches.[30−32] Tumor size was measured every 3 d using calipers, and the tumor volume was calculated using the formula: volume (mm^3) = 0.5 × [length (mm)] × [width (mm)]^2. Besides, the body weight of mice was measured every day. Mice were sacrificed with diethyl ether after 21 d of treatment, and then the tumors, hearts, liver, lung, and kidneys were collected, weighted, 4% paraformaldehyde-fixed, paraffin-embedded, and sectioned at a thickness of 4 μm for hematoxylin and eosin (H&E) staining. Additionally, sections of tumor tissue were also detected by TdT-mediated dUTP Nick-End Labeling (TUNEL) assay (Roche).

2.13. Ex Vivo Imaging Studies. 4T1-Bearing mice were obtained as described above. As the tumor volumes reached ~150 mm^3, DOX (5 mg/kg) and DOX@HNTs-PEG-FA (5 mg DOX equiv/kg) were injected into the tumor-bearing mice intravenously, respectively. At scheduled time points (1, 6, 10, and 24 h) post-intravenous-injection, tumor-bearing mice were killed. The tumor burden and the main organs were excised, washed, dried, and analyzed using the in vivo fluorescence imaging system (PerkinElmer).

2.14. Statistical Analysis. The data were presented as means ± standard deviation (SD). Statistical comparisons of data were performed using GraphPad Prism 6 (GraphPad Software) for one-way analysis of variance and a Tukey posthoc test. Values of all significant correlations (P < 0.05) were given with degree of significance indicated.

3. RESULTS AND DISCUSSION

3.1. Synthesize and Characterization of HNTs-PEG-FA. TEM images of short HNTs and HNTs-PEG-FA are shown in Figure 2A. Raw HNTs are usually inhomogeneous with a length from 100 nm to 2 μm.[33] To our surprise, after the ultrasonic scission, short HNTs emerge a smaller size with tube length below 200 nm, which is a benefit for the endocytosis of nanotubes. Furthermore, HNTs-PEG-FA still possesses a tubular structure with hollow lumen, which is because the electron beam of TEM can easily penetrate small organic matter and make the graft transparent. According to the AFM and SEM images of short HNTs and HNTs-PEG-FA in Figure 2B,C, it is hard to identify the differences in morphology before and after grafting of FA, which may be attributed to the low grafting ratio. It is generally recognized that the needlelike structure of HNTs is a benefit for entering cell via penetrating the plasma membrane directly.[34] As shown in Figure 2D, the size of HNTs-PEG-FA is 154 ± 7 nm, which is slightly higher than that of short HNTs (134 ± 8 nm).

Furthermore, the FTIR spectra of HNTs and HNTs-PEG-FA are shown in Figure 2E. Raw HNTs show typical absorption

DOI: 10.1021/acsanm.7b00087
ACS Appl. Nano Mater. 2018, 1, 595−608

peaks around 3695, 3620, 1025, and 910 cm^{-1}, which are assigned to O−H stretching peak of inner-surface hydroxyl groups, O−H stretching peak of inner hydroxyl groups, Si−O stretching peak of silica group, and O−H deformation of inner hydroxyl groups, respectively.[35] The absorption peak of 3000−2950 cm^{-1} is assigned to the C−H bond stretching of the grafted PEG in HNTs-PEG-FA. Besides, the peaks at 3695 and 3620 cm^{-1} assigned to O−H stretching peak of HNTs become weak in the HNTs-PEG-FA due to the grafting reaction. In addition, new peaks at 1405 and 1205 cm^{-1} can be attributed to the *p*-aminobenzoic acid moieties and C−O stretching bands of FA.[36,37] Raw HNTs do not contain N element, while N 1s peak appears in HNTs-PEG-FA, and C 1s peak is higher than that in raw HNTs through XPS analysis (Figure 2F). The atomic ratios in Figure S1 show that N element content of HNTs-PEG-FA is 2%. In addition, the ratio of C element increases from 15% to 77%, while the ratio of O element deceases from 54% to 12% after modification. The decrease of O content is due to the shielding effect of the grafted organics, and XPS can only measure the surface of nanoparticles with detection depth of several nanometers. The UV/vis absorption spectrum of HNTs-PEG-FA (Figure S2) shows that the absorption peak of FA (~280 nm) still exists, which further indicates that FA is successfully grafted onto HNTs. These results confirm that the chemical grafting of PEG and FA is successful.

Furthermore, the raw HNTs are negatively charged with −(24 ± 3) mV, which is consistent with the previous reports.[20,38] After PEG and FA are grafted, the zeta potential of HNTs is nearly neutralized, which also suggests the successful grafting of PEG and FA (Figure 2G). If the surface charges of nanoparticles are high (either positive or negative), they are more easily scavenged by macrophages. Tailoring the surface charges of nanoparticles can minimize the nonspecific interactions between nanoparticles and cells, which prevents the loss of nanoparticles in undesired locations.[39,40] As is well-known, the extent of hemolysis of nanoparticles is concentration-, porosity-, surface functionality-, and geometry-dependent.[41] Raw HNTs can cause abnormal destruction of red blood cells (hemolysis) with dose dependence,[42] and the phenomenon is decreased after surface modification such as chitosan grafting, chitosan oligosaccharide grafting, and polyethylenimine grafting.[23,26,28] In this study, HNTs-PEG-FA exhibits 1% hemolysis ratio at 1 mg/mL, while raw HNTs show 99% hemolysis ratio at the same concentration (Figure 2H). This phenomenon indicates that HNTs-PEG-FA is appropriate to apply as a drug carrier in intravenous injection.

3.2. DOX Loading and Release of HNTs-PEG-FA. The outer surface of HNTs-PEG-FA is hydrophilic, so the hydrophilic DOX can adsorb on the sidewalls of the modified HNTs. Also, the lumens of HNTs with ability of loading drug have been reported in previous studies.[43,44] HNTs are functionalized by FA-PEG moieties, and the sidewalls of HNTs are thus hydrophilic.[9,45] The loading of DOX on HNTs-PEG-FA is performed at neutral pH condition. In this situation, the hydrophilic DOX can locate both in the internal hollow space of the tubes and the sidewalls of the tubes.[44] The drug loading capacity and releasing dynamics of HNTs are related to drug/nanotubes weight ratio, the interactions of drug and HNTs, and adsorption conditions (time, temperature, pH value, etc.). DOX was loaded on HNTs via physical adsorption for 24 h under stirring.[26,46,47] Actually, the influence of the origins and surface property of HNTs on the loading and release of DOX was investigated.[46] It is found that HNTs and DOX can form a kind of complex via strong interactions, which is beneficial to high loading capacity and sustained release of DOX. However, it brings also side effect as low release percentage in their systems. The BET surface area of HNTs-PEG-FA is 48.7 m^2/g. The loading efficiency of DOX@HNTs-PEG-FA is calculated ~3%. Figure 3 shows the release curves of

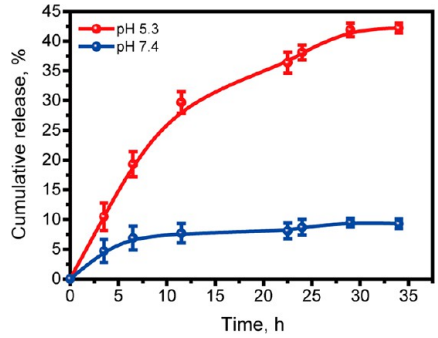

Figure 3. Drug release curves of DOX@HNTs-PEG-FA at pH 7.4 and 5.3.

DOX from DOX@HNTs-PEG-FA at different pH environment. Approximately 38% of DOX is released at 24 h in pH 5.3 condition, while only 9% is released in pH 7.4 conditions. Therefore, the release of DOX is pH-dependent, which is related to the protonation of NH_2 group of DOX. Besides, the low release ratio of DOX at pH 7.4 is a benefit for intravenous treatment of cancer, as the physiology pH of healthy human blood is 7.4. In contrast, the environment around the DOX@HNTs-PEG-FA drops to a lower pH of 5.5−6.0 in endosomes and approaches pH 4.5−5.0 in lysosomes.[45] Hence, DOX@HNTs-PEG-FA is relatively stable when circulating in the blood, and DOX can be retained in cytoplasm by endocytosis and rapidly releases from DOX@HNTs-PEG-FA when it is targeted to tumor sites where it is in a slightly acidic environment.[48] After it is targeted to the tumor cells, the DOX@HNTs-PEG-FA enters the cytoplasm, and DOX is released from these systems. In this situation, the amide bonds between FA and HNTs can break, and FA may leak due to the complicated cell inner environment in the presence of various enzymes. The leaking of FA in the cell has no harmful effect on the activities of cells, since FA is a type of vitamin. This has been proved in the following investigation.

3.3. Cytotoxicity of DOX@HNTs-PEG-FA. Figure 4 shows the cytotoxicity of L02 and MCF-7 cells treated with DOX, DOX@HNTs, and DOX@HNTs-PEG-FA. HNTs and HNTs-PEG-FA show greater than 90% cell viability toward both the normal cells and tumor cells even at a concentration of 500 μg/mL (Figure 4A,E). This indicates that HNTs and modified HNTs are biological friendly nanoparticles with low cytotoxicity. MCF-7 cells treated with DOX, DOX@HNTs, or DOX@HNTs-PEG-FA (Figure 4B) shows cytotoxicity in a dose-dependent manner ($P < 0.001$). It is noted that DOX@HNTs-PEG-FA shows enhanced inhibitory effects toward MCF-7 cell when compared to DOX treatment ($P < 0.001$). For example, the cell viability of DOX (10 μg/mL) is 55%, but DOX@HNTs-PEG-FA is 35% at the same DOX equivalent concentration (10 μg/mL). However, DOX@HNTs-PEG-FA shows no significant difference when compared to the DOX and DOX@HNTs treatments in the cells with negative expression of FA receptors, such as L02 cells (Figure 4F) and HepG2 (Figure S3). It has been well-recognized that

DOI: 10.1021/acsanm.7b00087
ACS Appl. Nano Mater. 2018, 1, 595−608

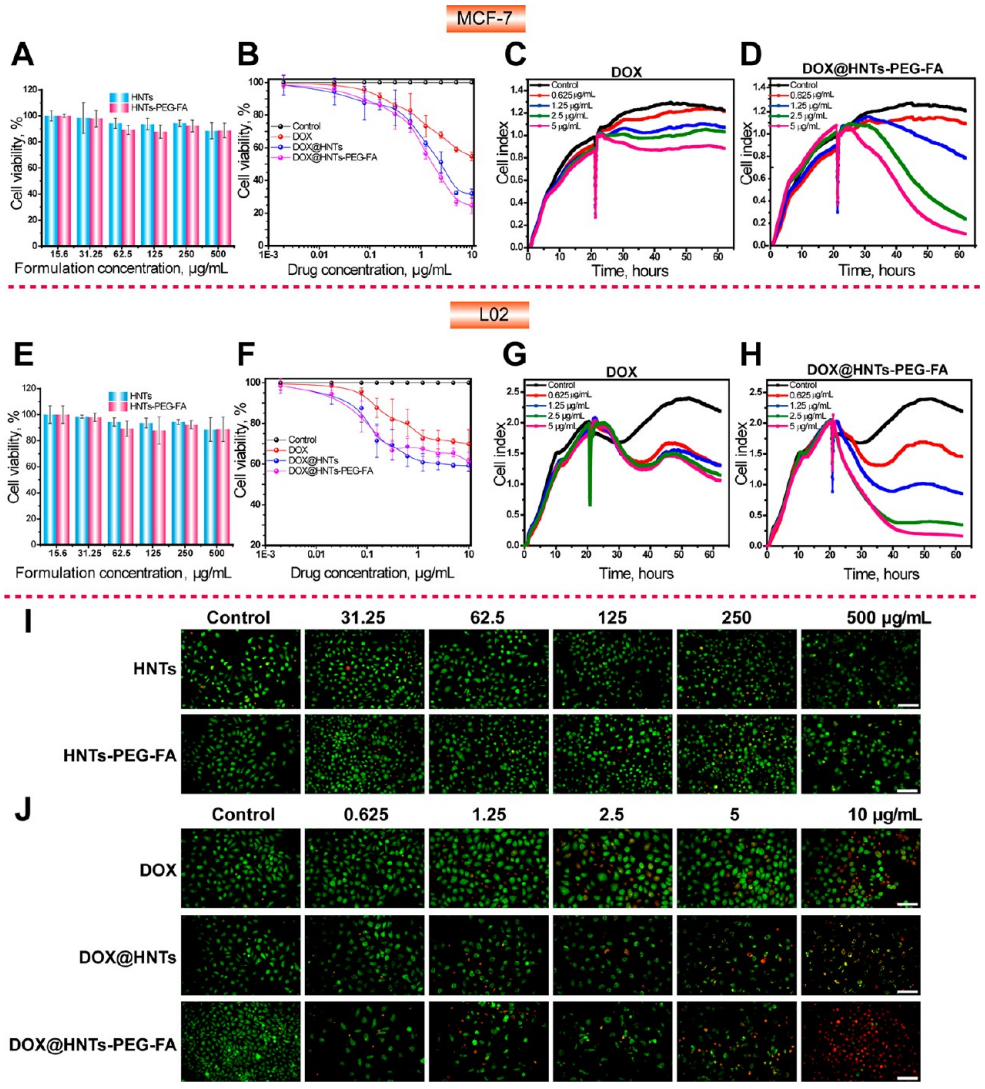

Figure 4. Cytotoxicity of DOX@HNTs-PEG-FA in vitro. The cell viability of (A, B) MCF-7 cells and (E, F) L02 cells treated with different concentrations of HNTs, HNTs-PEG-FA, DOX, DOX@HNTs, and DOX@HNTs-PEG-FA for 24 h (means ± SD, $n = 4$). The cell growth curve of (C, D) MCF-7 cells and (G, H) L02 cells treated with different concentrations (0.625, 1.25, 2.5, and 5 μg/mL) of DOX and DOX@HNTs-PEG-FA for 24 h. (I, J) The AO/EB staining of MCF-7 cells treated with different concentrations of HNTs, HNTs-PEG-FA, DOX, DOX@HNTs, and DOX@HNTs-PEG-FA for 24 h. Scale bar is 100 μm.

nanoparticles modified by folate are specifically targeting to the MCF-7 cell with positive FA receptor.[49,50] These results are a reminder that enhanced cytotoxicity of DOX@HNTs-PEG-FA is owing to the specific binding of FA and FA receptor in cytomembrane of MCF-7.

To further verify the result of cell viability, the real-time cell growth curve of L02 and MCF-7 cells treated with different concentrations (0.625, 1.25, 2.5, and 5 μg/mL) of DOX and DOX@HNTs-PEG-FA was recorded (Figure 4). DOX shows slight cytotoxicity to MCF-7 cells even when the DOX concentration is 5 μg/mL. The cell index of MCF-7 cells treated with DOX (5 μg/mL) at 50 h is ~0.9, while the control treatment is 1.3 (Figure 4C). The cell index of MCF-7 cells treated with different concentrations of DOX@HNTs-PEG-FA (drug concentration of 5 μg/mL) exhibits an obvious dose dependence, and the cell index is 0.2 at 50 h (Figure 4D). This strongly suggests that HNTs-PEG-FA exhibits a good entrapment and controlled release ability of drugs toward tumor cells. In comparison, HepG2 cells treated with DOX and DOX@HNTs-PEG-FA have not shown an apparent difference (Figure S3). The cell growth curves among these groups show no obvious difference, which is also due to the lack of FA receptor on their cytomembrane. The cell viability of human normal cells (L02 cells) treated with DOX and DOX@HNTs-PEG-FA at low concentration (<1.25 μg/mL, Figure 4G) decreases first, and then it increases for all groups. This suggests the capacity of resisting DOX in L02 cells. However, L02 cells treated with DOX@HNTs-PEG-FA also show a significantly decreased viability at the concentration of 1.25 μg/mL (Figure 4H). Therefore, DOX@HNTs-PEG-FA at low concentration does not result in significant damage to normal cells via intravenous injection.

Furthermore, the AO/EB staining fluorescence images of MCF-7 cells treated with HNTs and HNTs-PEG-FA are shown in Figure 4I,J. AO can enter cells with completed cell membrane and embed itself in DNA, displaying green fluorescence. On the contrary, EB only enters the cells with impaired cytomembrane and embeds itself in DNA, displaying orange fluorescence. MCF-7 cells treated with HNTs or HNTs-PEG-FA exhibit green fluorescence even in the concentration

DOI: 10.1021/acsanm.7b00087
ACS Appl. Nano Mater. 2018, 1, 595−608

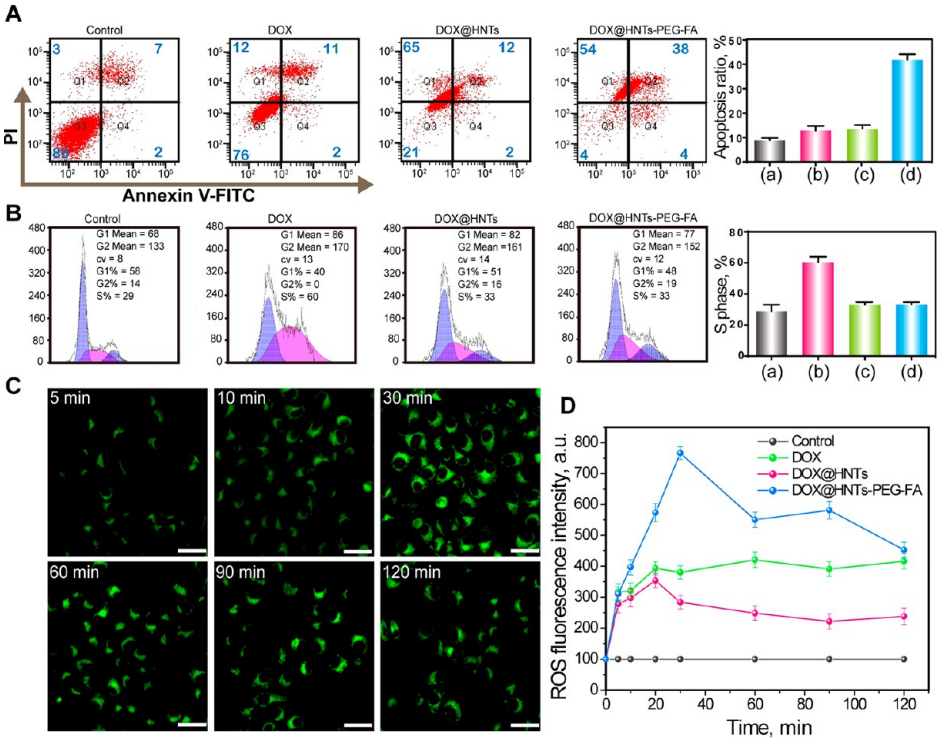

Figure 5. Effects of DOX@HNTs-PEG-FA on apoptosis in MCF-7 Cells. (A) Apoptosis and (B) cell cycle arrest of MCF-7 cells treated with (a) PBS, (b) DOX, (c) DOX@HNTs, and (d) DOX@HNTs-PEG-FA (DOX equivalent concentration was 5 μg/mL) for 10 and 24 h, respectively, were investigated by flow cytometer. (C) The ROS fluorescence image and (D) the quantitative ROS fluorescence intensity of MCF-7 cells treated with DOX@HNTs-PEG-FA at specific time was detected by fluorescence microplate. Scale bar is 50 μm. The values are represented as mean ± SD (n = 3).

of 500 μg/mL. It is illustrated that HNTs and HNTs-PEG-FA have cellular compatibility with negligible influence on the cell viability. Intriguingly, MCF-7 cells treated with DOX, DOX@HNTs, or DOX@HNTs-PEG-FA show noticeable differences by fluorescence images. DOX treatment shows great green fluorescence but less red in the most regions at different concentrations, reflecting a small number of dead cells. In contrast, DOX@HNTs-PEG-FA (the drug concentration of 10 μg/mL) treatment exhibits more orange and red with little green fluorescence, suggesting the apoptosis or cell death. These results demonstrate that DOX@HNTs-PEG-FA is more effective for promoting cell death compared to DOX and DOX@HNTs. In all, HNTs-PEG-FA can be a novel carrier for delivering DOX to cells.

3.4. Effects of DOX@HNTs-PEG-FA on Apoptosis in MCF-7 Cells. To investigate the mechanism of DOX@HNTs-PEG-FA in enhanced killing ability toward cancer cells, apoptosis assay, cell cycle assay, and ROS level were analyzed. Figure 5A shows the apoptosis effect of MCF-7 cells treated with control, DOX, DOX@HNT, and DOX@HNTs-PEG-FA (DOX equivalent concentration was 5 μg/mL) for 10 h was detected by flow cytometer. It is known that Q2 and Q4 quadrants represent the late apoptosis and early apoptosis, respectively. The apoptosis ratio significantly increases in DOX@HNTs-PEG-FA group (42%) when compared to control treatment and pristine DOX treatment (13%). This result confirms that DOX@HNTs-PEG-FA leads to the death of MCF-7 cells through apoptosis pathway.

To further explore the apoptotic mechanism of DOX and DOX@HNTs-PEG-FA, cell cycle was determined by flow cytometer (Figure 5B). It has been reported that DOX can embed in the DNA and break DNA, which prevents the synthesis of mRNA and consequently leads to the cell death. DOX can kill the cells in each cycle, but it is most sensitive in the S phase.[51] In Figure 5B, the S phase of pristine DOX treatment (60%) in 24 h significantly increases, while DOX@HNTs and DOX@HNTs-PEG-FA treatments show remarkable fall compared to DOX treatment (P < 0.001). So, DOX@HNTs-PEG-FA can induce death of cancer cells via another mechanism not only the effect of S phase-induced apoptosis. Furthermore, the ROS level of nanocarrier is investigated. ROS are well-known to be produced from the normal cellular oxygen metabolism and mainly include hydrogen superoxide, peroxide, and hydroxyl radicals. ROS are associated with apoptosis induced by chemotherapeutic agents and radiotherapy.[52] Generally, ROS level is balanced in normal cells. ROS were involved in the initiation phase of apoptosis contributing to cell death signaling such as by activating p53 and MAPK/AKT signal pathways. The ROS level of DOX@HNTs-PEG-FA in MCF-7 cell is increased dramatically first and reaches to peak at 30 min. Because of the antioxidant ability of cells, ROS level is decreased after 30 min. The tendency is similar to previous studies.[53,54] However, the ROS level of DOX@HNTs-PEG-FA group is higher than other groups at different times (Figure 5C,D). ROS are mostly produced by mitochondria, and the excess ROS can induce mitochondrial DNA mutations, damage the mitochondrial respiratory chain, alter membrane permeability, and influence Ca^{2+} homeostasis and mitochondrial defense systems.[55] Owing to the lack of histone protection and mitochondrial DNA near to the ROS produced sites, mitochondrial DNA damage is more significant than that of nuclear DNA.[56] All these results reveal that DOX@HNTs-

DOI: 10.1021/acsanm.7b00087
ACS Appl. Nano Mater. 2018, 1, 595−608

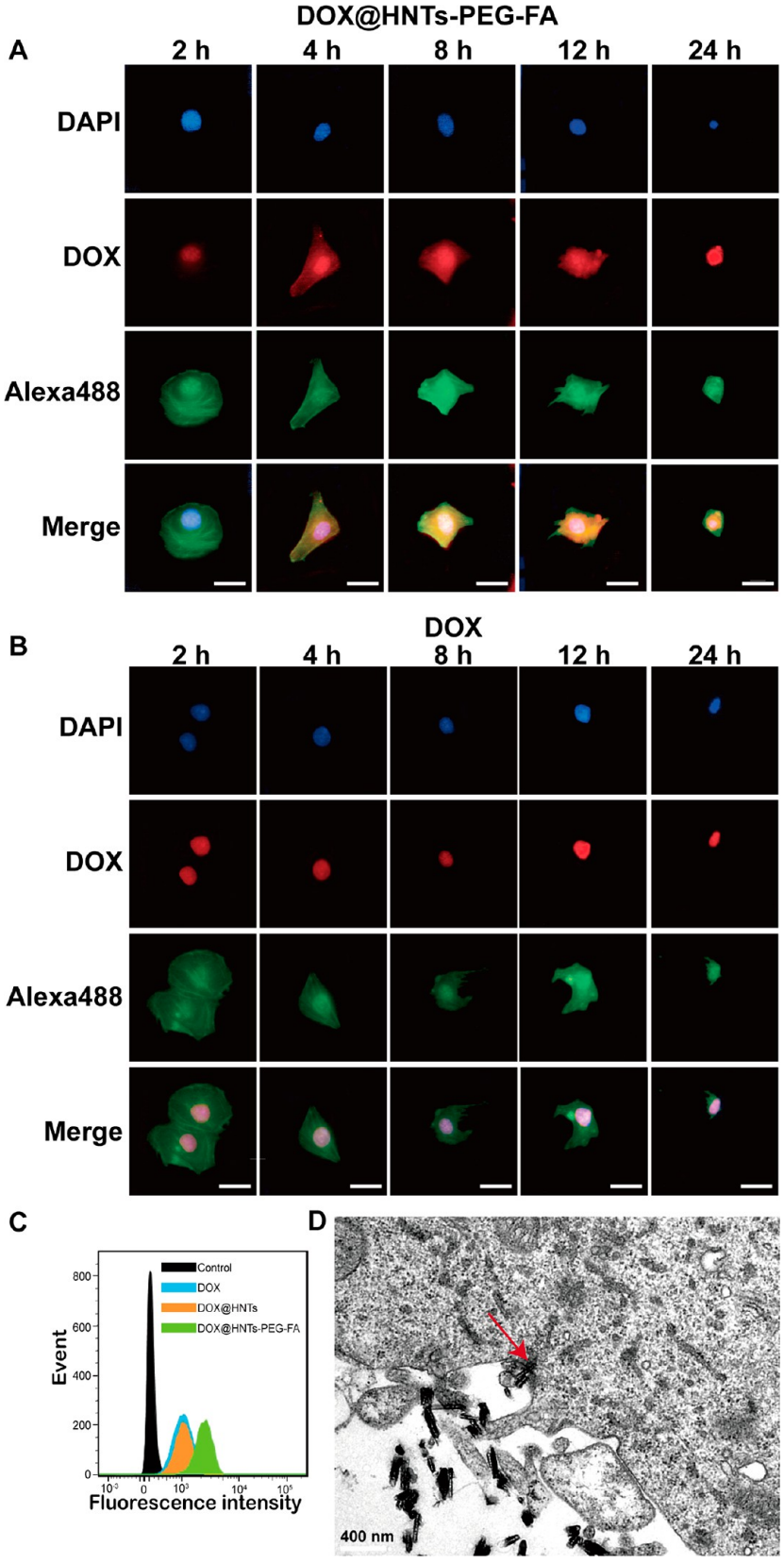

Figure 6. Uptake process of DOX@HNTs-PEG-FA by MCF-7 cells. The fluorescence images of (A) DOX@HNTs-PEG-FA and (B) DOX in MCF-7 cells were gained by fluorescent microscope. Scale bar is 50 μm. (C) Quantification fluorescence intensity of DOX in MCF-7 cells treated with DOX, DOX@HNTs, and DOX@HNTs-PEG-FA for 4 h was analyzed by flow cytometer. Scale bar is 400 nm. (D) The cell uptake process of HNTs-PEG-FA by MCF-7 cells was detected by TEM, and the red arrow indicates that HNTs are uptaken by cell.

DOI: 10.1021/acsanm.7b00087
ACS Appl. Nano Mater. 2018, 1, 595−608

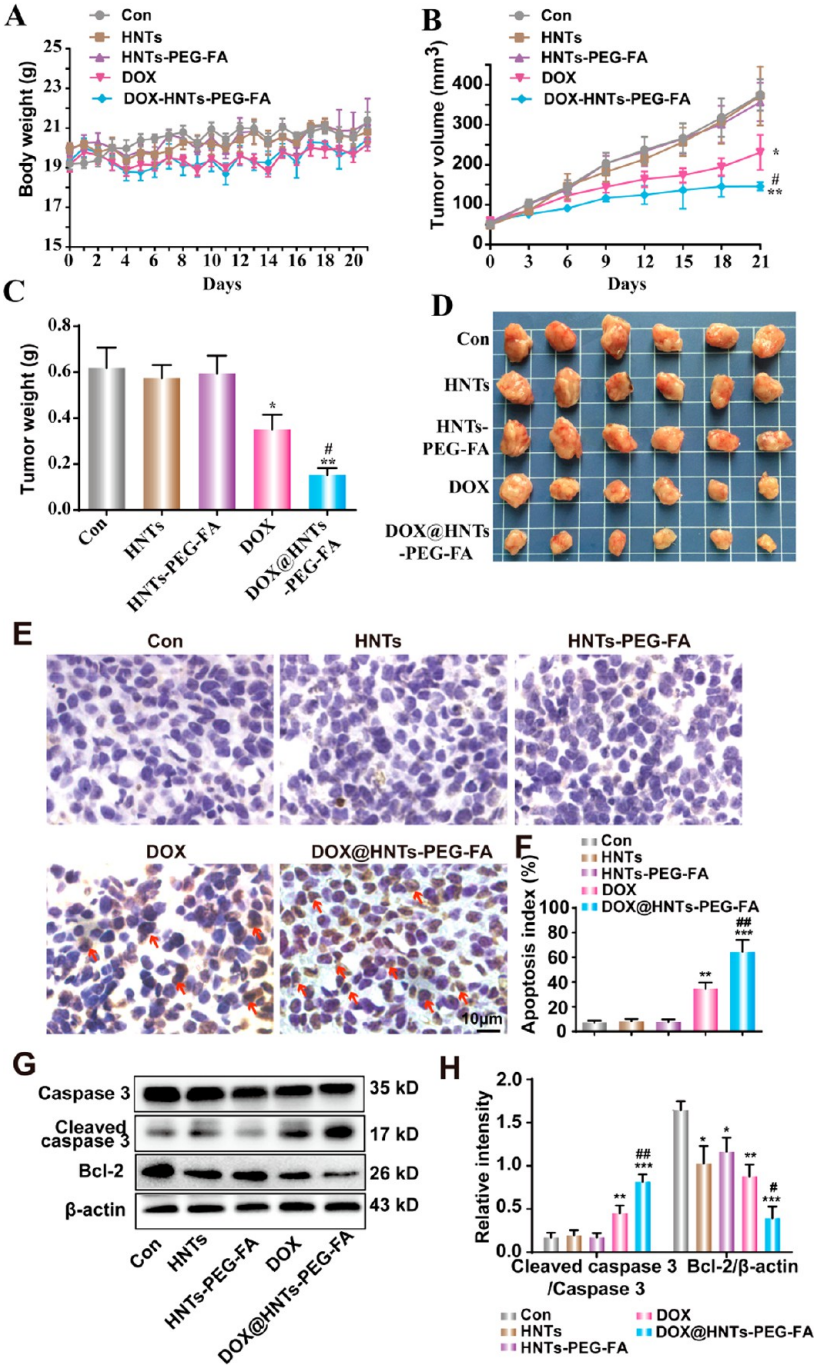

Figure 7. Antitumor effects of DOX@HNTs-PEG-FA in 4T1-bearing mice. (A) Body weight and (B) tumor growth curves of mice treated with saline, HNTs, HNTs-PEG-FA, DOX, and DOX@HNTs-PEG-FA (5 mg DOX equiv/kg) via intravenous injection. (C) Tumor weight and (D) photographs of excised 4T1 solid tumor from different groups on the 22nd day. (E) Representative photographs of tumor sections examined by TUNEL assay. TUNEL-positive cell nuclei (brown spots) were observed. (F) The number of apoptosis cells in different groups was counted in five random fields in a blinded manner. (G, H) Protein expression of caspase-3, cleaved caspase-3, and Bcl-2 in tumor tissue was detected by western blotting. The scale bars represent 10 μm. The values are represented as mean ± SD (n = 6). $^{*}P < 0.05$, $^{**}P < 0.01$, $^{***}P < 0.001$ vs control; $^{\#}P < 0.05$, $^{\#\#}P < 0.01$ vs DOX.

PEG-FA can effectively promote the apoptosis of tumor cell than pristine DOX via both mitochondrial damage and nuclei attack.

3.5. Uptake of DOX@HNTs-PEG-FA by MCF-7 Cells. The fluorescence images of MCF-7 cells treated with DOX@HNTs-PEG-FA and DOX at different times (2, 4, 8, 12, and 24 h) illustrating the uptake process are shown in Figure 6A,B. DOX@HNTs-PEG-FA is uptaken by MCF-7 cells gradually, and DOX released from DOX@HNTs-PEG-FA exists both in cytoplasm and nucleus before 12 h. In contrast, the pristine DOX is rapidly targeted in nucleus as early as 2 h due to the free mobility of DOX. DOX is intercalated with DNA and RNA in the nuclei. The drug restrained in the cytoplasm of the DOX@HNTs-PEG-FA group can enhance the anticancer efficiency via both the mitochondrial injury and nuclei injury mechanisms.[26,57] The morphology of cells changes as time with

DOI: 10.1021/acsanm.7b00087
ACS Appl. Nano Mater. 2018, 1, 595−608

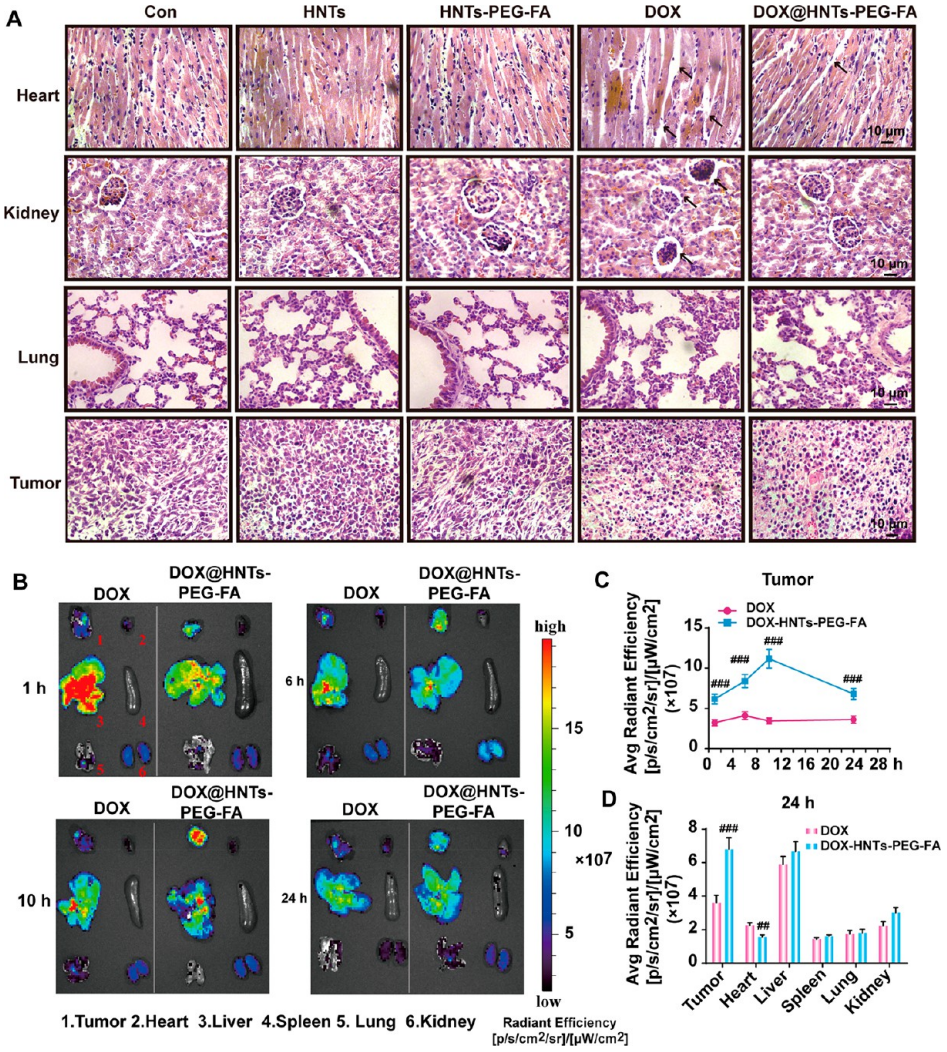

Figure 8. Tumor-targeted effect of DOX@HNTs-PEG-FA in 4T1-bearing mice. (A) H&E staining of tumor, heart, kidney, and lung slices from 4T1-bearing mice on the 22nd day after different treatments. The arrows in the heart sections indicate certain cardiomyocytes ruptured and scattered; the arrows in kidney sections indicate the deformation necrosis of glomerulus. The scale bars represent 10 μm. (B) DOX fluorescence images of different organs (1. Tumor, 2. Heart, 3. Liver, 4. Spleen, 5. Lung, 6. Kidney) from tumor-bearing mice at indicated time points (1, 6, 10, and 24 h) postadministration of DOX and DOX@HNTs-PEG-FA. (C) Quantification of DOX fluorescence of tumor tissues at indicated time points (1, 6, 10, and 24 h). (D) Quantification of DOX fluorescence of interested tissues (tumor, heart, liver, spleen, lung, and kidney) at 24 h. The values are represented as mean ± SD (n = 6). $^{\#\#}P < 0.01$, $^{\#\#\#}P < 0.001$ vs DOX.

distorted and ruptured cytomembrane at 8 h. Then the cytoplasm outflows from cytomembrane, resulting in a small nucleus and cytoplasm at 24 h.

Figure 6C shows quantification fluorescence intensity in MCF-7 cells after treated with DOX, DOX@HNTs, and DOX@HNTs-PEG-FA. The fluorescence intensity of DOX@HNTs-PEG-FA obviously increases compared to the DOX and DOX@HNTs treatments. It is likewise attributed to the fact that FA can react with FA receptor in the cytomembrane. DOX@HNTs-PEG-FA can easily enter to cells, and the DOX amount of this treatment obviously increases compared to DOX and DOX@HNTs treatments. Therefore, FA in HNTs-PEG-FA keeps the binding activity and specificity to FA receptor, which promotes the cellular uptake through receptor-mediated endocytosis. This is a coupled process in which selected extracellular proteins or peptides are first bound to specific cell surface receptors and then rapidly internalized by cells.

As we know, nanoparticles were size-dependent cellular uptake,[34,58] and the size of DOX@HNTs-PEG-FA is 154 ± 7 nm. To directly observe the uptake of DOX@HNTs-PEG-FA by MCF-7, TEM image of MCF-7 cells is shown in Figure 6D. HNTs are chemically composed with Al, Si, and O elements, so the electron density is relatively high. In addition, HNTs show unique tubular microstructure. So, it is easy to distinguish the nanotubes from cellular component using TEM. Clearly, tubular-like particles or their aggregates are distributed evenly around the cell membrane as shown in Figure 6D. Single HNTs can directly penetrate the plasma membrane into the cytoplasm (indicated by the red arrow). In contrast to single HNTs, aggregated HNTs may have a tendency to enter cells through endocytosis. The internalization of other nanotubes or nanosheets through endocytosis and direct penetration was also observed by TEM technology.[59−61]

3.6. Antitumor Effects of DOX@HNTs-PEG-FA in 4T1-Bearing Mice. In our previous work on drug-loaded HNTs for in vivo tumor therapy,[26] the anticancer effect of DOX@HNTs-

DOI: 10.1021/acsanm.7b00087
ACS Appl. Nano Mater. 2018, 1, 595−608

g-COS was confirmed in 4T1-bearing mice model via intratumor injection. To further investigate the natural HNTs as anticancer drug carrier for targeting tumor therapy, the effects of DOX@HNTs-PEG-FA on antitumor activity of 4T1-bearing mice via tail intravenous injection are studied. Different treatments show no significant influence on body weight (Figure 7A). As expected, DOX ($P < 0.05$) and DOX@HNTs-PEG-FA ($P < 0.01$) treatments significantly reduce the tumor volume and tumor weight in 4T1-bearing mice by comparing to the control group, while HNTs and HNTs-PEG-FA treatments have no significant change (Figure 7B,D). Furthermore, compared to DOX treatment, DOX@HNTs-PEG-FA treatment significantly decreases both tumor volume and tumor weight ($P < 0.05$). These data indicate that DOX@HNTs-PEG-FA has a remarkable antitumor effect in vivo, which is consistent with the in vitro results.

Subsequently, the apoptosis index in tumor tissue was examined by TUNEL assay (Figure 7E). Compared to control group, both DOX@HNTs-PEG-FA ($P < 0.001$) and DOX treatment ($P < 0.01$) induce significant apoptosis in tumor tissue. The number of $TUNEL^+$ nuclei in DOX@HNTs-PEG-FA group (65%) is significantly higher than in DOX group (35%; $P < 0.01$; Figure 7F). The result agrees with apoptosis analysis in MCF-9 cell in vitro and further confirms that DOX@HNTs-PEG-FA can induce significant apoptosis in tumor cell. Besides, the expression levels of caspase-3, cleaved caspase-3, and Bcl-2 proteins in tumor tissue are examined by western blotting (Figure 7G,H). In mammalian cells, caspase-3 normally exists as an inactive precursor (35 kDa), while it is converted to an active heterodimer (17 kDa) when apoptosis happens.[62] Besides, Bcl-2 is an integral membrane protein located mainly on the outer membrane of mitochondria. Overexpression of Bcl-2 prevents cells from undergoing apoptosis in response to a variety of stimuli.[63] A significant increased cleavage of caspase-3 is observed ($P < 0.01$), and the expression of antiapoptotic protein Bcl-2 is notably decreased in DOX@HNTs-PEG-FA group ($P < 0.05$) compared to the DOX group. Collectively, these data confirm that DOX@HNTs-PEG-FA enhances the antitumor efficacy by influencing the expression of apoptosis-related pathway in vivo. These results are in agreement with our previous study on the antitumor ability of chitosan oligosaccharide-grafted HNTs as a DOX carrier.[26]

3.7. Tumor-Targeted Efficiency of DOX@HNTs-PEG-FA in 4T1-Bearing Mice. The histological analysis shows that DOX@HNTs-PEG-FA induces significantly more tumor necrosis than does DOX (Figure 8A), while the control, HNTs, and HNTs-PEG-FA groups show no significant changes. In contrast to DOX@HNTs-PEG-FA treated group and control group, DOX treatment results in obvious heart damage (cardiomyocytes rupture and scatter) and slight nephrotoxicity (deformation necrosis of glomerulus), which corresponds to their side effects. As for the lung tissue, there are no significant changes among all the treatments. The results suggest that DOX@HNTs-PEG-FA can target 4T1 breast cancer cells, leading to high therapy efficacy with markedly reduced systemic toxicity. On the basis of the facts that 4T1 cell is used as a model of FA receptor-expressed cell surface,[64−66] so DOX@HNTs-PEG-FA may effectively target the solid tumor tissue. To verify this assumption, DOX fluorescence of the major tissues (tumor, heart, liver, spleen, lung, and kidney) excised from tumor-bearing mice at indicated time points (1, 6, 10, and 24 h) postadministration of DOX and DOX@HNTs-PEG-FA was detected by fluorescence imaging system (Figure 8B). Intriguingly, the results (Figure 8C) reveal that DOX fluorescence in tumor significantly accumulates in 1 h and reaches the maximum at 10 h after the administration of DOX@HNTs-PEG-FA, while the DOX treatment reaches the maximum at only 2 h ($P < 0.001$). Additionally, DOX@HNTs-PEG-FA treatment reveals a considerably higher DOX fluorescence intensity in the tumor than in normal tissues including heart, spleen, lung, and kidney after 24 h postadministration (Figure 8D and Figure S4). By comparison, mice treated with DOX show weaker DOX fluorescence in tumor, which is likely due to the inadequate drug release within tumor. These results suggest that DOX@HNTs-PEG-FA can effectively target and release the drugs to 4T1 breast cancer in mice.

Although HNTs are nondegradable materials, they can be used as anticancer drug carrier owing to their very low toxicity levels of HNTs in vivo. One may expect that chronic inflammatory reactions induced by HNTs do not occur. Little is known about the mechanisms of low toxicity of HNTs; however, HNTs reside among the safest nanoscale materials. In vivo tests of HNTs employing *Paramecium caudatum* protists, *Caenorhabditis elegans* nematodes, and zebrafish embryos demonstrate very low cytotoxicity.[67]

4. CONCLUSIONS

HNTs are conjugated with PEG and FA for effectively delivering DOX to breast cancer. The length of HNTs is first shortened to ∼200 nm by ultrasonic scission. HNTs-PEG-FA shows particle size and zeta potential of 154 ± 7 nm and 1 ± 0.3 mV, respectively. FTIR and XPS results confirm the successful grafting of FA and PEG onto HNTs. DOX can be loaded on HNTs-PEG-FA via physical adsorption. DOX is released from DOX@HNTs-PEG-FA up to 35 h in an acidic environment (pH = 5.3), while it is relatively stable in neutral conditions. DOX@HNTs-PEG-FA nanodelivery system can restrain proliferation and induce death of MCF-7 cells with positive FA receptor, while it shows relative low cytotoxicity toward the L02 cells with negative FA receptor. DOX@HNTs-PEG-FA can produce more ROS in MCF-7 cells, which lead to the apoptosis. The uptake of DOX@HNTs-PEG-FA by MCF-7 cells can happen both through endocytosis and direct penetration mechanism. DOX@HNTs-PEG-FA group effectively inhibits solid tumor growth, while it reduces heart toxicity of DOX. Cleaved caspase-3 protein levels of 4T1 tumor treated with DOX@HNTs-PEG-FA are significantly higher than the control groups. DOX@HNTs-PEG-FA group reveals a considerably higher DOX fluorescence intensity in tumor than in normal tissues including heart, spleen, lung, and kidney. All these results suggest that the FA-conjugated HNTs may be designed to be a novel drug delivery platform for targeting therapy of breast via intravenous injection.

■ ASSOCIATED CONTENT

Supporting Information

The Supporting Information is available free of charge on the ACS Publications website at DOI: 10.1021/acsanm.7b00087.

The atomic percent of HNTs and HNTs-PEG-FA, UV/vis absorption spectrum of HNTs and HNTs-PEG-FA, cell viability of HNTs, HNTs-PEG-FA, DOX, DOX@HNTs, and DOX@HNTs-PEG-FA after 24 h of incubation and cell growth curve of DOX and DOX@

DOI: 10.1021/acsanm.7b00087
ACS Appl. Nano Mater. 2018, 1, 595−608

HNTs-PEG-FA toward HepG2, DOX fluorescence quantification of the major tissues excised from tumor-bearing mice at indicated time points (1, 6, 10, and 24 h) postadministration of DOX and DOX@HNTs-PEG-FA, summary of the important results and conclusion (PDF)

AUTHOR INFORMATION

Corresponding Authors

*E-mail: rongronghe@jnu.edu.cn. (R.-R.H.)
*E-mail: liumx@jnu.edu.cn. (M.L.)

ORCID

Mingxian Liu: 0000-0002-5466-3024

Author Contributions

§These authors contributed equally to this work.

Notes

The authors declare no competing financial interest.

ACKNOWLEDGMENTS

This work was financially supported by National High Technology Research and Development Program of China (2015AA020915), the National Natural Science Foundation of China (Grant Nos. 51473069, 81622050, and 51502113), and the Guangdong Natural Science Funds for Distinguished Young Scholar (Grant No. S2013050014606), Science and Technology Program of Guangzhou, China (Nos. 2013J4100100 and 201610010026), Guangdong Special Support Program (2014TQ01C127 and 2014TQ01R229), the Fundamental Research Funds for the Central Universities (21615204) and Guangdong Province Ocean and Fisheries Bureau-Key Technology Research and Development Program (A201701A02). We thank Z.-Q. Liu and L.-L. Lu from International Institute for Translational Chinese Medicine (Guangzhou Univ. of Chinese Medicine) for providing the in vivo fluorescence imaging analysis.

REFERENCES

(1) Blum, R. H.; Carter, S. K. Adriamycin: A New Anticancer Drug with Significant Clinical Activity. *Ann. Intern. Med.* **1974**, *80*, 249−259.

(2) Lefrak, E. A.; Pit'ha, J.; Rosenheim, S.; Gottlieb, J. A. A Clinicopathologic Analysis of Adriamycin Cardiotoxicity. *Cancer* **1973**, *32*, 302−314.

(3) Von Hoff, D. D.; Layard, M. W.; Basa, P.; Davis, H. L.; Von Hoff, A. L.; Rozencweig, M.; Muggia, F. M. Risk Factors for Doxorubicin-Lnduced Congestive Heart Failure. *Ann. Intern. Med.* **1979**, *91*, 710−717.

(4) Lee, C. C.; Gillies, E. R.; Fox, M. E.; Guillaudeu, S. J.; Fréchet, J. M.; Dy, E. E.; Szoka, F. C. A Single Dose of Doxorubicin-Functionalized Bow-Tie Dendrimer Cures Mice Bearing C-26 Colon Carcinomas. *Proc. Natl. Acad. Sci. U. S. A.* **2006**, *103*, 16649−16654.

(5) Qiao, J.; Mu, X.; Qi, L.; Deng, J.; Mao, L. Folic Acid-Functionalized Fluorescent Gold Nanoclusters with Polymers as Linkers for Cancer Cell Imaging. *Chem. Commun.* **2013**, *49*, 8030−8032.

(6) Leamon, C. P.; Reddy, J. A. Folate-Targeted Chemotherapy. *Adv. Drug Delivery Rev.* **2004**, *56*, 1127−1141.

(7) Sudimack, J.; Lee, R. J. Targeted Drug Delivery Via the Folate Receptor. *Adv. Drug Delivery Rev.* **2000**, *41*, 147−162.

(8) Dhar, S.; Liu, Z.; Thomale, J.; Dai, H.; Lippard, S. J. Targeted Single Wall Carbon Nanotube Mediated Pt (Iv) Prodrug Delivery Using Folate as a Homing Device. *J. Am. Chem. Soc.* **2008**, *130*, 11467.

(9) Wolski, P.; Nieszporek, K.; Panczyk, T. Pegylated and Folic Acid Functionalized Carbon Nanotubes as Ph Controlled Carriers of Doxorubicin. Molecular Dynamics Analysis of the Stability and Drug Release Mechanism. *Phys. Chem. Chem. Phys.* **2017**, *19*, 9300−9312.

(10) Niu, L. Y.; Meng, L. J.; Lu, Q. H. Folate-Conjugated Peg on Single Walled Carbon Nanotubes for Targeting Delivery of Doxorubicin to Cancer Cells. *Macromol. Biosci.* **2013**, *13*, 735−744.

(11) Bharali, D. J.; Lucey, D. W.; Jayakumar, H.; Pudavar, H. E.; Prasad, P. N. Folate-Receptor-Mediated Delivery of Inp Quantum Dots for Bioimaging Using Confocal and Two-Photon Microscopy. *J. Am. Chem. Soc.* **2005**, *127*, 11364−11371.

(12) Landmark, K. J.; DiMaggio, S.; Ward, J.; Kelly, C.; Vogt, S.; Hong, S.; Kotlyar, A.; Myc, A.; Thomas, T. P.; Penner-Hahn, J. E.; et al. Synthesis, Characterization, and in Vitro Testing of Superparamagnetic Iron Oxide Nanoparticles Targeted Using Folic Acid-Conjugated Dendrimers. *ACS Nano* **2008**, *2*, 773−783.

(13) Li, J. C.; Zheng, L. F.; Cai, H. D.; Sun, W. J.; Shen, M. W.; Zhang, G. X.; Shi, X. Y. Polyethyleneimine-Mediated Synthesis of Folic Acid-Targeted Iron Oxide Nanoparticles for in Vivo Tumor Mr Imaging. *Biomaterials* **2013**, *34*, 8382−8392.

(14) Xu, L. Y.; Bai, Q. M.; Zhang, X.; Yang, H. Folate-Mediated Chemotherapy and Diagnostics: An Updated Review and Outlook. *J. Controlled Release* **2017**, *252*, 73−82.

(15) Sonvico, F.; Mornet, S.; Vasseur, S.; Dubernet, C.; Jaillard, D.; Degrouard, J.; Hoebeke, J.; Duguet, E.; Colombo, P.; Couvreur, P. Folate-Conjugated Iron Oxide Nanoparticles for Solid Tumor Targeting as Potential Specific Magnetic Hyperthermia Mediators: Synthesis, Physicochemical Characterization, and in Vitro Experiments. *Bioconjugate Chem.* **2005**, *16*, 1181−1188.

(16) Joussein, E.; Petit, S.; Churchman, J.; Theng, B.; Righi, D.; Delvaux, B. Halloysite Clay Minerals−a Review. *Clay Miner.* **2005**, *40*, 383−426.

(17) Price, R. R.; Lvov, Y.; Gaber, B. P. In-Vitro Release Characteristics of Tetracycline Hcl, Khellin and Nicotinamide Adenine Dineculeotide from Halloysite; a Cylindrical Mineral. *J. Microencapsulation* **2001**, *18*, 713−722.

(18) Lvov, Y. M.; Shchukin, D. G.; Mohwald, H.; Price, R. R. Halloysite Clay Nanotubes for Controlled Release of Protective Agents. *ACS Nano* **2008**, *2*, 814−820.

(19) Ruiz-Hitzky, E.; Ariga, K.; Lvov, Y. M. *Bio-Inorganic Hybrid Nanomaterials: Strategies, Synthesis, Characterization and Applications;* John Wiley & Sons: 2008.

(20) Levis, S.; Deasy, P. Characterisation of Halloysite for Use as a Microtubular Drug Delivery System. *Int. J. Pharm.* **2002**, *243*, 125−134.

(21) Levis, S.; Deasy, P. Use of Coated Microtubular Halloysite for the Sustained Release of Diltiazem Hydrochloride and Propranolol Hydrochloride. *Int. J. Pharm.* **2003**, *253*, 145−157.

(22) Cavallaro, G.; Lazzara, G.; Massaro, M.; Milioto, S.; Noto, R.; Parisi, F.; Riela, S. Biocompatible Poly (N-Isopropylacrylamide)-Halloysite Nanotubes for Thermoresponsive Curcumin Release. *J. Phys. Chem. C* **2015**, *119*, 8944−8951.

(23) Liu, M.; Chang, Y.; Yang, J.; You, Y.; He, R.; Chen, T.; Zhou, C. Functionalized Halloysite Nanotube by Chitosan Grafting for Drug Delivery of Curcumin to Achieve Enhanced Anticancer Efficacy. *J. Mater. Chem. B* **2016**, *4*, 2253−2263.

(24) Chao, C.; Liu, J.; Wang, J.; Zhang, Y.; Zhang, B.; Zhang, Y.; Xiang, X.; Chen, R. Surface Modification of Halloysite Nanotubes with Dopamine for Enzyme Immobilization. *ACS Appl. Mater. Interfaces* **2013**, *5*, 10559−10564.

(25) Chao, C.; Zhang, B.; Zhai, R.; Xiang, X.; Liu, J.; Chen, R. Natural Nanotube-Based Biomimetic Porous Microspheres for Significantly Enhanced Biomolecule Immobilization. *ACS Sustainable Chem. Eng.* **2014**, *2*, 396−403.

(26) Yang, J.; Wu, Y.; Shen, Y.; Zhou, C.; Li, Y.-F.; He, R.-R.; Liu, M. Enhanced Therapeutic Efficacy of Doxorubicin for Breast Cancer Using Chitosan Oligosaccharide-Modified Halloysite Nanotubes. *ACS Appl. Mater. Interfaces* **2016**, *8*, 26578−26590.

(27) Rong, R.; Xu, X.; Zhu, S.; Li, B.; Wang, X.; Tang, K. Facile Preparation of Homogeneous and Length Controllable Halloysite Nanotubes by Ultrasonic Scission and Uniform Viscosity Centrifugation. *Chem. Eng. J.* **2016**, *291*, 20−29.

DOI: 10.1021/acsanm.7b00087
ACS Appl. Nano Mater. 2018, 1, 595−608

(28) Long, Z.; Zhang, J.; Shen, Y.; Zhou, C.; Liu, M. Polyethyleneimine Grafted Short Halloysite Nanotubes for Gene Delivery. *Mater. Sci. Eng., C* **2017**, *81*, 224−235.
(29) Joo, Y.; Jeon, Y.; Lee, S. U.; Sim, J. H.; Ryu, J.; Lee, S.; Lee, H.; Sohn, D. Aggregation and Stabilization of Carboxylic Acid Functionalized Halloysite Nanotubes (Hnt-Cooh). *J. Phys. Chem. C* **2012**, *116*, 18230−18235.
(30) Li, H.; Cui, Y.; Sui, J.; Bian, S.; Sun, Y.; Liang, J.; Fan, Y.; Zhang, X. Efficient Delivery of Dox to Nuclei of Hepatic Carcinoma Cells in the Subcutaneous Tumor Model Using Ph-Sensitive Pullulan-Dox Conjugates. *ACS Appl. Mater. Interfaces* **2015**, *7*, 15855−15865.
(31) Hao, Y.; Zheng, C.; Wang, L.; Hu, Y.; Guo, H.; Song, Q.; Zhang, H.; Zhang, Z.; Zhang, Y. Covalent Self-Assembled Nanoparticles with Ph-Dependent Enhanced Tumor Retention and Drug Release for Improving Tumor Therapeutic Efficiency. *J. Mater. Chem. B* **2017**, *5*, 2133−2144.
(32) Li, Y.; Xu, X.; Zhang, X.; Li, Y.; Zhang, Z.; Gu, Z. Tumor-Specific Multiple Stimuli-Activated Dendrimeric Nanoassemblies with Metabolic Blockade Surmount Chemotherapy Resistance. *ACS Nano* **2017**, *11*, 416−429.
(33) Liu, M.; Jia, Z.; Jia, D.; Zhou, C. Recent Advance in Research on Halloysite Nanotubes-Polymer Nanocomposite. *Prog. Polym. Sci.* **2014**, *39*, 1498−1525.
(34) Kostarelos, K.; Lacerda, L.; Pastorin, G.; Wu, W.; Wieckowski, S.; Luangsivilay, J.; Godefroy, S.; Pantarotto, D.; Briand, J.-P.; Muller, S.; et al. Cellular Uptake of Functionalized Carbon Nanotubes Is Independent of Functional Group and Cell Type. *Nat. Nanotechnol.* **2007**, *2*, 108−113.
(35) Madejová, J. Ftir Techniques in Clay Mineral Studies. Vib. *Vib. Spectrosc.* **2003**, *31*, 1−10.
(36) He, Y.; Wang, X.; Jin, P.; Zhao, B.; Fan, X. Complexation of Anthracene with Folic Acid Studied by Ftir and Uv Spectroscopies. Spectrochim. *Spectrochim. Acta, Part A* **2009**, *72*, 876−879.
(37) Sun, C.; Sze, R.; Zhang, M. Folic Acid-Peg Conjugated Superparamagnetic Nanoparticles for Targeted Cellular Uptake and Detection by Mri. *J. Biomed. Mater. Res., Part A* **2006**, *78A*, 550−557.
(38) Liu, M.; Zhang, Y.; Wu, C.; Xiong, S.; Zhou, C. Chitosan/Halloysite Nanotubes Bionanocomposites: Structure, Mechanical Properties and Biocompatibility. *Int. J. Biol. Macromol.* **2012**, *51*, 566−575.
(39) Davis, M. E.; Shin, D. M.; et al. Nanoparticle Therapeutics: An Emerging Treatment Modality for Cancer. *Nat. Rev. Drug Discovery* **2008**, *7*, 771−782.
(40) Jang, J.-t.; Jeong, S.; Seo, J.-w.; Kim, M.-C.; Sim, E.; Oh, Y.; Nam, S.; Park, B.; Cheon, J. Ultrathin Zirconium Disulfide Nanodiscs. *J. Am. Chem. Soc.* **2011**, *133*, 7636−7639.
(41) Yu, T.; Malugin, A.; Ghandehari, H. Impact of Silica Nanoparticle Design on Cellular Toxicity and Hemolytic Activity. *ACS Nano* **2011**, *5*, 5717−5728.
(42) Liu, H.-Y.; Du, L.; Zhao, Y.-T.; Tian, W.-Q. Vitro Hemocompatibility and Cytotoxicity Evaluation of Halloysite Nanotubes for Biomedical Application. *J. Nanomater.* **2015**, *2015*, 1.
(43) Yuan, P.; Southon, P. D.; Liu, Z.; Kepert, C. J. Organosilane Functionalization of Halloysite Nanotubes for Enhanced Loading and Controlled Release. *Nanotechnology* **2012**, *23*, 375705.
(44) Abdullayev, E.; Price, R.; Shchukin, D.; Lvov, Y. Halloysite Tubes as Nanocontainers for Anticorrosion Coating with Benzotriazole. *ACS Appl. Mater. Interfaces* **2009**, *1*, 1437−1443.
(45) Gillies, E. R.; Frechet, J. M. J. Ph-Responsive Copolymer Assemblies for Controlled Release of Doxorubicin. *Bioconjugate Chem.* **2005**, *16*, 361−368.
(46) Li, L.; Fan, H.; Wang, L.; Jin, Z. Does Halloysite Behave Like an Inert Carrier for Doxorubicin? *RSC Adv.* **2016**, *6*, 54193−54201.
(47) Zhang, Y.; Long, M.; Huang, P.; Yang, H.; Chang, S.; Hu, Y.; Tang, A.; Mao, L. Intercalated 2d Nanoclay for Emerging Drug Delivery in Cancer Therapy. *Nano Res.* **2017**, *10*, 1−11.
(48) Liu, J.; Huang, Y.; Kumar, A.; Tan, A.; Jin, S.; Mozhi, A.; Liang, X.-J. Ph-Sensitive Nano-Systems for Drug Delivery in Cancer Therapy. *Biotechnol. Adv.* **2014**, *32*, 693−710.
(49) Qi, L.; Guo, Y.; Luan, J.; Zhang, D.; Zhao, Z.; Luan, Y. Folate-Modified Bexarotene-Loaded Bovine Serum Albumin Nanoparticles as a Promising Tumor-Targeting Delivery System. *J. Mater. Chem. B* **2014**, *2*, 8361−8371.
(50) Pi, J.; Jin, H.; Liu, R.; Song, B.; Wu, Q.; Liu, L.; Jiang, J.; Yang, F.; Cai, H.; Cai, J. Pathway of Cytotoxicity Induced by Folic Acid Modified Selenium Nanoparticles in Mcf-7 Cells. *Appl. Microbiol. Biotechnol.* **2013**, *97*, 1051−1062.
(51) Del Bino, G.; Darzynkiewicz, Z. Camptothecin, Teniposide, or 4′-(9-Acridinylamino)-3-Methanesulfon-M-Anisidide, but Not Mitoxantrone or Doxorubicin, Induces Degradation of Nuclear DNA in the S Phase of Hl-60 Cells. *Cancer Res.* **1991**, *51*, 1165−1169.
(52) Pelicano, H.; Carney, D.; Huang, P. Ros Stress in Cancer Cells and Therapeutic Implications. Drug Resist. *Drug Resist. Updates* **2004**, *7*, 97−110.
(53) Huang, Y.; He, L.; Song, Z.; Chan, L.; He, J.; Huang, W.; Zhou, B.; Chen, T. Phycocyanin-Based Nanocarrier as a New Nanoplatform for Efficient Overcoming of Cancer Drug Resistance. *J. Mater. Chem. B* **2017**, *5*, 3300−3314.
(54) He, L.; Zeng, L.; Mai, X.; Shi, C.; Luo, L.; Chen, T. Nucleolin-Targeted Selenium Nanocomposites with Enhanced Theranostic Efficacy to Antagonize Glioblastoma. *J. Mater. Chem. B* **2017**, *5*, 3024−3034.
(55) Guo, C.; Sun, L.; Chen, X.; Zhang, D. Oxidative Stress, Mitochondrial Damage and Neurodegenerative Diseases. *Neural Regener. Res.* **2013**, *8*, 2003.
(56) Wiseman, H.; Halliwell, B. Damage to DNA by Reactive Oxygen and Nitrogen Species: Role in Inflammatory Disease and Progression to Cancer. *Biochem. J.* **1996**, *313*, 17.
(57) Xiong, H.; Du, S.; Ni, J.; Zhou, J.; Yao, J. Mitochondria and Nuclei Dual-Targeted Heterogeneous Hydroxyapatite Nanoparticles for Enhancing Therapeutic Efficacy of Doxorubicin. *Biomaterials* **2016**, *94*, 70−83.
(58) Zhang, S.; Li, J.; Lykotrafitis, G.; Bao, G.; Suresh, S. Size-Dependent Endocytosis of Nanoparticles. *Adv. Mater.* **2009**, *21*, 419.
(59) Mu, Q.; Su, G.; Li, L.; Gilbertson, B. O.; Yu, L. H.; Zhang, Q.; Sun, Y.-P.; Yan, B. Size-Dependent Cell Uptake of Protein-Coated Graphene Oxide Nanosheets. *ACS Appl. Mater. Interfaces* **2012**, *4*, 2259−2266.
(60) Mu, Q.; Broughton, D. L.; Yan, B. Endosomal Leakage and Nuclear Translocation of Multiwalled Carbon Nanotubes: Developing a Model for Cell Uptake. *Nano Lett.* **2009**, *9*, 4370−4375.
(61) Dzamukova, M. R.; Naumenko, E. A.; Lvov, Y. M.; Fakhrullin, R. F. Enzyme-Activated Intracellular Drug Delivery with Tubule Clay Nanoformulation. *Sci. Rep.* **2015**, *5*.10.1038/srep10560
(62) Nicholson, D. W.; Ali, A.; Thornberry, N. A.; Vaillancourt, J. P.; et al. Identification and Inhibition of the Ice/Ced-3 Protease Necessary for Mammalian Apoptosis. *Nature* **1995**, *376*, 37.
(63) Yang, J.; Liu, X.; Bhalla, K.; Kim, C. N.; Ibrado, A. M.; Cai, J.; Peng, T.-I.; Jones, D. P.; Wang, X.; et al. Prevention of Apoptosis by Bcl-2: Release of Cytochrome C from Mitochondria Blocked. *Science* **1997**, *275*, 1129−1132.
(64) Prabaharan, M.; Grailer, J. J.; Pilla, S.; Steeber, D. A.; Gong, S. Folate-Conjugated Amphiphilic Hyperbranched Block Copolymers Based on Boltorn (R) H40, Poly(L-Lactide) and Poly(Ethylene Glycol) for Tumor-Targeted Drug Delivery. *Biomaterials* **2009**, *30*, 3009−3019.
(65) Prabaharan, M.; Grailer, J. J.; Steeber, D. A.; Gong, S. Thermosensitive Micelles Based on Folate-Conjugated Poly(N-Vinylcaprolactam)-Block-Poly(Ethylene Glycol) for Tumor-Targeted Drug Delivery. *Macromol. Biosci.* **2009**, *9*, 744−753.
(66) Alibolandi, M.; Abnous, K.; Hadizadeh, F.; Taghdisi, S. M.; Alabdollah, F.; Mohammadi, M.; Nassirli, H.; Ramezani, M. Dextran-Poly Lactide-Co-Glycolide Polymersomes Decorated with Folate-Antennae for Targeted Delivery of Docetaxel to Breast Adenocarcinima in Vitro and in Vivo. *J. Controlled Release* **2016**, *241*, 45−56.
(67) Kryuchkova, M.; Danilushkina, A.; Lvov, Y.; Fakhrullin, R. Evaluation of Toxicity of Nanoclays and Graphene Oxide in Vivo: A Paramecium Caudatum Study. *Environ. Sci.: Nano* **2016**, *3*, 442−452.

DOI: 10.1021/acsanm.7b00087
ACS Appl. Nano Mater. 2018, 1, 595−608